Journal of Sol-Gel Science and Technology (2024) 112:768–775
https://doi.org/10.1007/s10971-024-06572-w

ORIGINAL PAPER

"Tuning density and morphology of organic-inorganic hybrid-silica aerogels through precursor dilution for lightweight applications"

K. Steffens[1] · D. Bialuschewski[1] · B. Milow[1,2]

Received: 19 June 2024 / Accepted: 24 September 2024 / Published online: 11 October 2024

Abstract

Organic-inorganic hybrid-silica aerogels can be made of methyltrimethoxysilane (MTMS, $CH_3Si(OCH_3)_3$) and dimethyldimethoxysilane (DMDMS, $Si(OCH_3)_2(CH_3)_2$) in a typical sol-gel process yielding flexible and hydrophobic structures. In this work, MTMS and DMDMS were condensed with an increasing amount of water, leading to a decrease in the final materials density from ~ 0.110 g cm^{-3} down to ~0.066 g cm^{-3}. The gels were synthesized in a one-pot synthesis and dried under ambient pressure conditions at 80 °C. While the topology of the network remained intact, the size of secondary particles decreased from roughly 8.2 to 3.3 µm. The inter-particle neck thickness remained unaffected with increasing aging time for higher dilutions. The measured thermal conductivities were all in similar range (~ 32.5 mW (m K)$^{-1}$ at 25 °C), showing very good insulation characteristics. In general, higher diluted samples exhibited increasing softness and decreasing Young's modulus, even with increased aging times. Overall, our optimized recipe leads to hydrophobic aerogels with ultralow densities while demonstrating very low thermal conductivity and a flexible mechanical performance.

Graphical Abstract

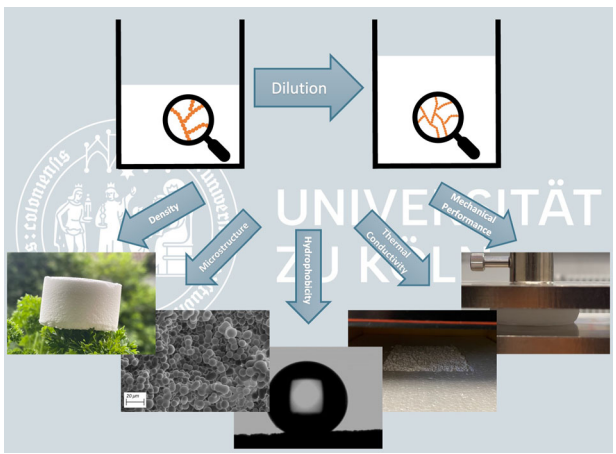

Keywords density reduction · heat insulation · hybrid materials · sol-gel-process · flexible aerogel

✉ B. Milow
Barbara.Milow@dlr.de

[1] University of Cologne, Institute of Inorganic Chemistry, Greinstraße 4 – 6, 50939 Köln, Germany

[2] German Aerospace Center, Institute of Materials Research, Linder Höhe, 51147 Köln, Germany

Highlights

- Synthesis of flexible and lightweight hybrid-silica aerogel.
- Density reduction without loss of good thermal insulation properties.
- No change in hydrophobicity and therefore no water-uptake.

1 Introduction

The demand for advanced nanostructured materials that combine exceptional mechanical properties with efficient thermal insulation has fueled ongoing research in materials science and engineering. Thermal insulation materials play a pivotal role in the aviation industry, where they are essential for ensuring the safety, efficiency, and comfort of the passengers and the crew. In the high-altitude environment of aircraft, temperatures can fluctuate dramatically, from freezing cold at higher altitudes to blistering heat on the ground in summer [1, 2]. Proper thermal insulation helps to regulate the internal temperature of the aircraft, ensuring that passengers remain comfortable and that sensitive electronic systems operate optimally [3, 4]. Furthermore, insulation materials protect critical components, such as fuel lines and hydraulic systems, from temperature extremes that could lead to malfunction or failure. By maintaining a stable and controlled environment within the aircraft, these materials contribute to both safety and energy efficiency, reducing the strain on heating and cooling systems and the aircraft's environmental footprint. Therefore, high value thermal insulation materials are essential for the aviation industry, guaranteeing passenger comfort, system reliability, and overall flight safety [5].

In this context, silica aerogels with their remarkable properties, namely low density, thermal conductivity and high sound absorption, all a result of their highly nanostructured porous network, are ideal candidates for aeronautical applications [6–10]. While pure silica aerogels are very brittle and difficult to handle, adapting the sol-gel process and utilizing organic-inorganic alkoxysilane precursors can result in hybrid-materials with a high mechanical flexibility and a good hydrophobicity while still retaining a remarkable insulation performance [11, 12]. They were first investigated in 2011 by Hayase et al. [13] and are based on methyltrimethoxysilane (MTMS) and dimethoxydimethylsilane (DMDMS). In this context, the choice of precursor plays a significant role. Among the various possible precursor combinations [9], MTMS and DMDMS have remained the most utilized choice due to their compatibility and the ability to fine-tune the properties of resulting hybrid-silica aerogels.

The synthesis of these flexible hybrid aerogels depends on several fundamental parameters. One of these is the precursor-to-water ratio, which can be modified during the sol-gel process. With appropriate variation, the density of the final aerogel product can be systematically controlled, thus influencing the final aerogel properties. One challenge is exploring the balance between mechanical adaptability and thermal efficiency, as both properties are directly dependent on the solid fraction in the material.

While many other studies in literature focused on the precursors-ratio (MTMS:DMDMS) [14–18] or catalysts concentration [15, 19], there is only one publication by Hayase et al. on the precursor-to-water-ratio for MTMS/DMDMS co-precursor systems [20]. With a MTMS:DMDMS-ratio of 1:0.33 they synthesized samples with densities of 0.22 – 0.07 g cm^{-3} and investigated the microstructure, the mechanical and thermal properties in the application related field of cryogenic thermal insulators. In contrast, we were starting our study with a recipe patented by our group at the *German Aerospace Center (DLR)* [21] in 2023 with MTMS:DMDMS-ratio of 1:0.67 which should result in higher hydrophobicity due to the increased number of CH_3-groups in the porous network. We further modified the synthesis route by varying the precursor-to-solvent ratios with the aim to decrease the materials density allowing the material to be used as possible aircraft insulation material. Therefore, mechanical, thermal, chemical and morphological properties of the samples were analyzed in detail for several sample geometries (from small cylindrically shaped samples up to bigger mats) and are discussed in this work.

2 Experimental

2.1 Materials

The precursors used were methyltrimethoxysilane (MTMS) and dimethyldimethoxysilane (DMDMS), obtained from *abcr GmbH*, Germany. Acetic acid (AcOH) was purchased from *Fisher Scientific GmbH*, Germany and cetyltrimethylammonium chloride solution (CTAC, 25 wt.% in H_2O) from *Sigma-Aldrich GmbH*, Germany. Urea was received from *Merck KGaA*, Germany. All chemicals were used as received. All sol-gel-solutions were prepared from purified water. For the washing steps, ethanol from *Fisher Scientific GmbH*, Germany and isopropanol from *Sigma-Aldrich GmbH*, Germany were used, both technical grades.

2.2 Preparation

The synthesis consists of four main steps, namely, hydrolysis, condensation, aging and washing/drying, which were done in a simple one-pot reaction as follows.

Table 1 Synthesis recipes for 380 g (~350 mL) of total solution for reference sample (a) and modified samples (b – i). Samples b, d, f, h represent the "dilution all"-series; samples c, e, g, i represent the "water"-series

Sample	H_2O:MTMS-ratio	Aging [d]	H_2O [g]	Urea [g]	AcOH [µL]	MTMS [g]	CTAC [g]	DMDMS [g]
a	39.65	1	177.99	74.39	71	42.50	59.91	25.13
b	50.00	1	204.82	64.51	62	36.86	51.95	21.79
c	50.00	1	184.80	77.24	74	34.99	62.20	20.69
d	55.00	3	215.38	60.62	58	34.63	48.82	20.48
e	55.00	3	187.30	78.28	75	32.24	63.04	19.06
f	60.00	7	224.74	57.18	55	32.67	46.04	19.32
g	60.00	7	189.43	79.17	76	29.89	63.75	17.67
h	65.00	7	233.09	54.10	52	30.91	43.57	18.28
i	65.00	7	191.27	79.94	77	27.86	64.37	16.47

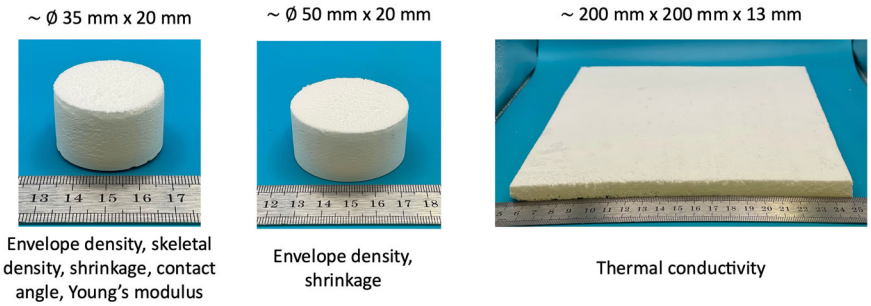

Fig. 1 Overview of the three different synthesized sample dimensions with the respective characterization technique they were used for

First, the necessary amounts (cf. Table 1) of distilled water and urea were mixed, and heated up to 50 °C. For the hydrolysis, acetic acid was added, followed by MTMS and CTAC. The solution was mixed for 15 min at 50 °C. Then DMDMS was added and mixed for another 45 min. Afterwards the sol was transferred to closed vessels and placed in an oven at 80 °C for the listed time of gelation/condensation and aging (cf. Table 1). Before drying the obtained wet gels were transferred into fresh solvents for washing to remove unreacted chemicals and the surfactant CTAC. Due to limited diffusion washing was carried out for 24 h each following the order: water, ethanol, water, water, isopropanol. After that the samples were finally dried out of isopropanol under ambient pressure at 80 °C for 24 h in an oven.

The samples were named and categorized as follows: Sample **a** represents the standard reference sample synthesized according to literature [21]. Samples **b, d, f** and **h** represent the "all"-series with increasing water:MTMS-ratio, which means that all used chemicals (urea, AcOH, CTAC) with exception of the precursors were raised by the same level as the water. Samples **c, e, g** and **i** represent the "water"-series with increasing water:MTMS-ratio, which means that only the amount of water used during the synthesis was increased without changing the other ratios.

For the different characterization techniques several sample geometries were synthesized (cf. Fig. 1).

2.3 Characterization

The envelope density ρ_{env} of the cylindrical shaped samples was measured by caliper and scale, calculating the volume, and dividing it by the mass of the sample weight with an analytical balance. The skeletal density ρ_{skel} was measured with helium pycnometer AccuPyc® II 1340 from *Micromeritics*^{TM}, Germany. Each measurement consists of ten purging cycles to remove air out of the sample and sample-chamber followed by ten measurement cycles. From both densities, the porosity Φ of the material was calculated using Eq. 1. The radial shrinkage S_r was calculated by comparing the diameter of the container used for synthesis with the final aerogel's diameter.

$$\Phi = 1 - \frac{\rho_{skel}}{\rho_{env}} \tag{1}$$

To analyze the samples microstructure images were taken with a scanning electron microscope (SEM) Merlin from *Carl Zeiss*, Germany at an acceleration voltage of 2–3 kV and a working distance of 7–10 mm. Before observation the samples were sputtered with platinum for 100 s. The particle sizes were determined from these SEM images with the help of the software ImageJ.

To demonstrate the samples hydrophobicity the water drop contact angle θ_c was determined by Drop Shape Analyzer DSA 100 from *KRÜSS*, Germany. For this, a

Table 2 Envelope and skeletal density of samples with their respecting calculated porosity and measured radial shrinkage. The error of all skeletal density measurements is ± 0.01 g cm^{-3}

Sample	H_2O:MTMS-ratio	Envelope density ρ_{env} [g cm^{-3}]		Skeletal density ρ_{skel} [g cm^{-3}]		Porosity Φ [%]		Radial shrinkage S_r [%]	
		all	water	all	water	all	water	all	water
a	39.65	0.106 ± 0.002		1.26		91.6		2.3 ± 0.5	
b / c	50.00	0.086 ± 0.003	0.089 ± 0.004	1.29	1.28	93.3	93.1	2.5 ± 0.7	2.0 ± 0.3
d / e	55.00	0.079 ± 0.002	0.086 ± 0.005	1.26	1.32	93.8	93.5	1.7 ± 0.5	3.2 ± 1.2
f / g	60.00	0.071 ± 0.005	0.077 ± 0.006	1.31	1.27	94.6	94.0	2.4 ± 1.2	3.0 ± 1.3
h / i	65.00	0.066 ± 0.003	0.073 ± 0.002	1.29	1.29	94.9	94.3	2.7 ± 0.9	2.2 ± 0.6

water droplet of 5.0 µL was placed on the samples surface and the contact angle was automatically determined.

The thermal conductivity was measured in the range of 0–60 °C by the heat flow meter apparatus HFM 436 Lambda from *NETZSCH*, Germany. The samples had a size of 200 × 200 mm^2 and a height of 13 mm.

Uniaxial compression testing was performed on cylindrical-shaped samples with dimensions of 34 mm in diameter and 20 mm in height on the universal testing machine *ZwickRoell* Z2.5, Germany equipped with 50 N load cell. All tests were conducted at a deformation rate of 10 mm min^{-1}. All investigated aerogels were subjected to compressive loading up to strain of 60% and then subsequently unloaded.

3 Results and discussion

3.1 Density, microstructure and surface chemistry

Table 2 shows the mean values for ρ_{env}, ρ_{skel}, Φ and S_r of all synthesized samples, per variation at minimum eight in two different cylindrical shapes (cf. Fig. 1). The errors were calculated as standard deviation from mean values. With higher amount of water, the samples resulted in lower envelope densities. For every dilution level the "all"-series shows slightly lower densities compared to the "water"-series. The lightest samples **h** exhibited a 38% lower density with 0.066 g cm^{-3} compared to references **a** having 0.106 g cm^{-3}. Skeletal density for all samples was observed in the same range of 1.26 to 1.32 g cm^{-3}. Since the solid composition of the final material (MTMS:DMDMS-ratio) is not varied, this result was expected. The porosity changes similar to the envelope density, as it increases with dilution. The measured radial shrinkage is 2 – 3% for all samples within their error.

Scanning electron images of the flexible silica aerogels are shown in Fig. 2. It can be observed that each sample consists of micrometer-sized spherical particles connected via inter-particle necks. The dilution of the precursors was leading to smaller particles, as the total mass, coming solely from the amount of precursor used, stays constant while the total volume was increased. The diameter of the particles was determined by averaging the size of 20 particles for each sample as shown in Table 3 (D_{SEM}). It decreases with increasing dilution of siloxane precursors from 8.2 µm for reference **a** down to 3.2 and 3.3 µm for samples **h** and **i**. Every level of dilution shows comparable morphology and particle diameters for each dilution in both "water" and "all"-series. Hayase et al. observed similar tendencies for a different MTMS:DMDMS-ratio [20]. The samples with water:MTMS-ratio of 65.00 both show a rougher particle surface (Fig. 2h, i). The thickness of inter-particle necks seems to be stable for all synthesized samples due to adjusted aging time from 1 up to 7 days for higher diluted samples. Higher diluted samples without increasing the aging time could not successfully be synthesized during the experiments due to their very fragile structure. While demolding and washing the samples break apart very easily. After longer aging the particle necks grow due to Ostwald ripening [22, 23] and the samples are able to withstand more external forces.

The water drop contact angles θ_c of the samples are listed in Table 3. The measured angles are in range from 129° up to 140° for all samples. These results lead to the assumption that the hydrophobicity of the final material is not influenced by the dilution of siloxane precursors during synthesis, as expected, as the amount of hydrophobic Si-CH_3 groups covering the surface should not be influenced due to the constant MTMS:DMDMS-ratio [24]. Figure 3 shows a 5.0 µL water droplet on top of reference sample **a**. The high hydrophobicity prevents the material from gaining weight due to moisture condensation, which would happen between aircraft takeoff and landing if used as insulation material [25–27].

3.2 Thermal properties

HFM studies were carried out in the range of 0 – 60 °C and are shown in Fig. 4. Samples **a** – **e** and **g** could be synthesized in the required dimensions of minimum 200 × 200 mm^2 in a special self-made mold (Fig. 4, right). Samples **f, h** and **i** were broken during washing steps due to their very fragile nature in big dimensions and could

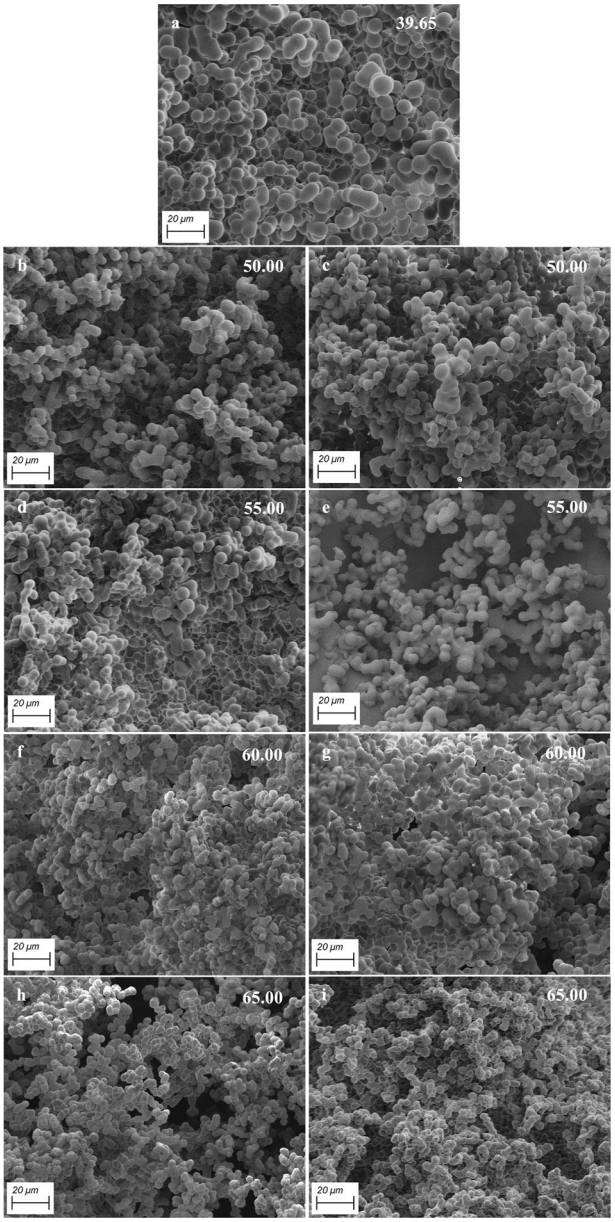

Fig. 2 Scanning electron microscope images derived from reference sample "**a**" and modified samples (**b–i**). The left column represents the "all"-series and the right column the "water"-series

therefore not be measured. In general, smaller samples are easier to handle. The thermal conductivity increases with higher temperatures for all samples, as expected [28–30]. The dilution seems to have no major influence on the measured thermal conductivities, since all pore sizes observed in the SEM pictures are much larger than the mean free path of air molecules and therefore are not reducing the thermal conductivity due to contribution of the gaseous phase. Within the expected precision of the system, all samples show similar values, which vary in range from minimum ~ 30 mW (m K)$^{-1}$ at 0 °C up to ~ 37 mW (m K)$^{-1}$ at 60 °C for all samples. Sample **g** with lowest density for all synthesized mats (0.077 g cm^{-3}) shows a thermal conductivity of ~ 32.5 mW (m K)$^{-1}$ at 25 °C, which is on the lower range. The measured conductivities could be confirmed with values from literature [20, 31].

Table 3 Mean particle size calculated from SEM images and water drop contact angle determined by drop shape analyzer

Sample	H_2O:MTMS-ratio	Mean particle size D_{SEM} [µm]		Water drop contact angle θ_c [°]	
		all	water	all	water
a	39.65	8.2 ± 1.2		136	
b/c	50.00	5.6 ± 1.0	5.3 ± 0.9	140	129
d/e	55.00	5.2 ± 0.8	4.7 ± 0.7	127	138
f/g	60.00	3.9 ± 0.6	3.9 ± 0.4	140	129
h/i	65.00	3.3 ± 0.5	3.4 ± 0.6	137	135

3.3 Mechanical properties

While classical silica aerogels show hard and brittle nature, organic-inorganic hybrids are soft and flexible. Therefore, the samples could be easily compressed uniaxially up to a strain (ε) of 60% (Fig. 5, right). After compression the samples were unloaded and immediately recovered to their original height without any visible damage. The measured stress-strain-curves are shown in Fig. 5. All samples show a linear-elastic behavior up to $\varepsilon < 20\%$.

From stress-strain-curves the Young's modulus E was calculated in linear range from 0 to 10% compression strain (Table 4). Reference **a** has the highest Young's modulus (7.89 kPa) compared to the diluted samples. Samples from "water"-series (**c, e, g, i**) show generally higher values than samples from "all"-series (**b, d, f, h**). Former show a decrease in Young's modulus with increasing water: MTMS-ratio from 5.22 to 3.23 kPa, for later no influence of dilution could be observed for calculated Young's modulus (~ 3 kPa). A decrease in Young's modulus with increasing dilution was expected because of the weaker solid backbone structure. The samples' elastic moduli are comparable to literature values [13, 31].

To study the influence of aging on the mechanical behavior of samples, reference sample **a** was additionally synthesized with three and seven days of aging. The resulting stress-strain-curves are presented in supporting information (cf. Fig. S2). It could be seen that differing the aging time can lead to slightly harder material.

4 Summary and conclusion

In this study, the density and morphology of flexible hybrid-silica aerogels is tuned by implementing an efficient dilution

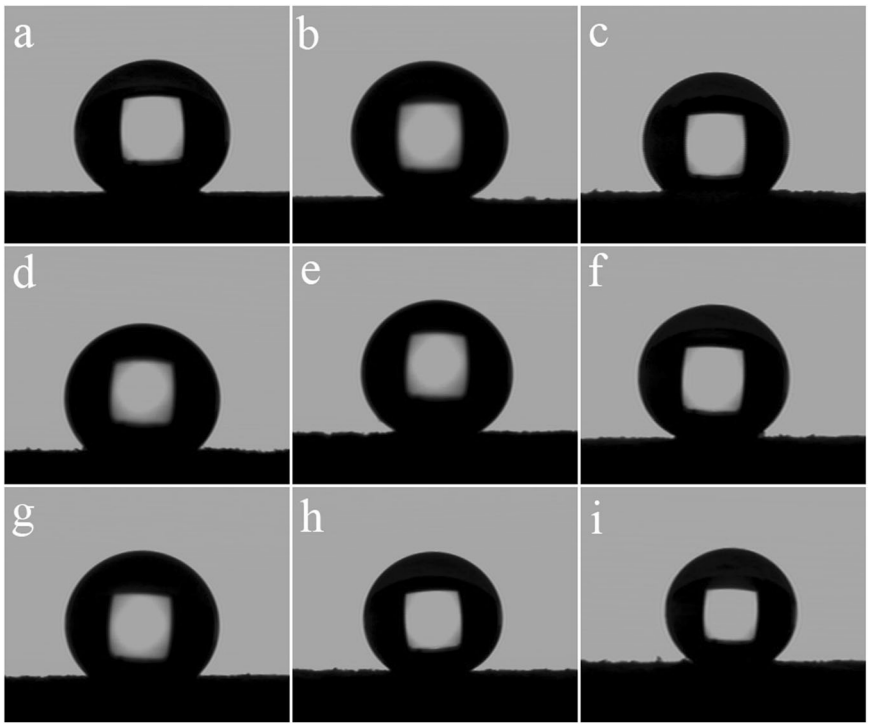

Fig. 3 Photograph of 5.0 µL water droplet on sample **a – i**. The contact angles determined for each sample are presented in Table 3

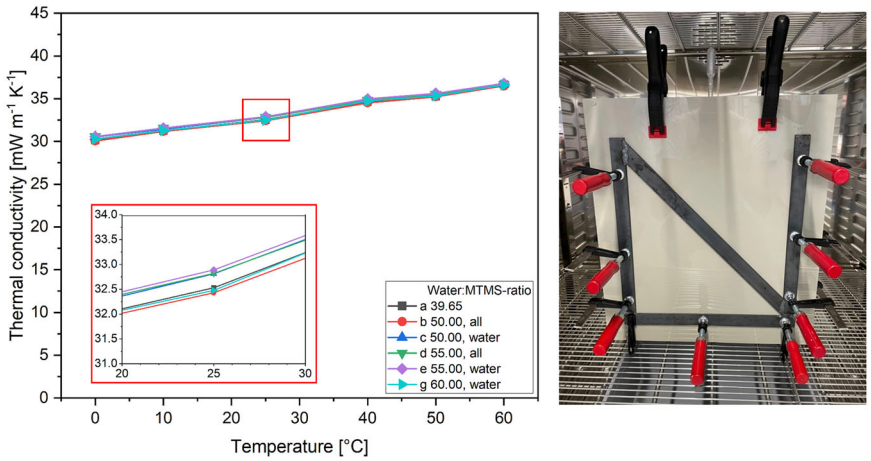

Fig. 4 Thermal conductivity of samples in temperature range of 0–60 °C (left) and special self-made mold for upright synthesis of samples in minimum dimensions of 200 × 200 mm^2 (right)

process of initial precursor system, targeted for lightweight-applications. To this end, the envelope and skeletal densities were investigated first, followed by analysis of their microstructure and the mean particle diameters via SEM images. The samples hydrophobicity was evaluated via water drop contact angle measurements. Next, the thermal properties of the samples were measured, and finally, uni-axial mechanical compression tests were performed.

The envelope density could be optimized to 0.066 g cm^{-3}, a 38% lower density compared to reference sample. It could be observed that the overall topology of the sample's microstructure did not change drastically by variation of the water:MTMS-ratio from 39.65 to 65.00. The mean particle size decreased from 8.2 to 3.3 µm but the inter-particle neck thickness seemed not to be influenced by increasing aging time (range of 1 to 7 days) for the higher diluted samples. The low thermal conductivity of the synthesized samples (~ 32.5 mW (m K)$^{-1}$ at 25 °C) seemed also not to be affected in the investigated dilution range. During mechanical testing, a decrease in Young's modulus from 7.9 to 2.8 kPa could be observed.

The aerogels in general have a similar performance to the reference sample and values reported in literature but show a much lower density and are better suited for lightweight applications. While other studies focused on a single property such as high hydrophobicity, low thermal

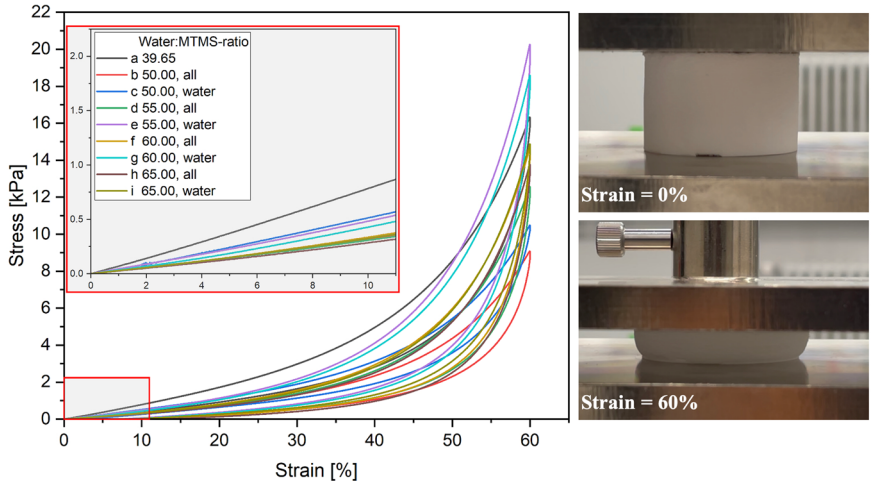

Fig. 5 Uniaxial stress-strain-curve (left) and sample images of compression testing at 0 and 60% strain (right). After testing the samples spring back to their original height. More detailed single stress-strain-curves are shown in supporting information (Fig. S1)

Table 4 Young's Modulus *E* calculated in linear range of stress-strain-curves from 0 to 10% strain for samples a – i

Sample	H_2O:MTMS-ratio	Young's modulus *E* [kPa]	
		all	water
a	39.65	7.89	
b/c	50.00	3.08	5.22
d/e	55.00	3.03	4.81
f/g	60.00	3.36	4.30
h/i	65.00	2.82	3.23

conductivity, good mechanical properties or low density, we achieved a material which combines all properties for the prospective application in aviation. Further experiments to upscale to larger sample geometries need to be conducted in the future to investigate the mechanical and the thermal performance of the material at lower temperatures down to −50 °C. Combining the diluted aerogel material with woven fiber matrix could improve the bendability and allow to roll-up the material for distribution.

Supplementary information The online version contains supplementary material available at https://doi.org/10.1007/s10971-024-06572-w.

Acknowledgements The authors gratefully acknowledge funding by the Federal Ministry of Economic Affairs and Climate Action (BMWK) and its Aviation Research Program "LuFo VI-1" ("MULTIKABIN", FKZ: 20Q1908C). The authors are grateful to Rebekka Probst from German Aerospace Center Cologne for her assistance with SEM characteriza-tion, Prof. Dr. Annette M. Schmidt and Benoît Rhein from University of Cologne for their assistance with compression testing and providing the facility. We would also like to thank Ass.-Prof. Dr. Andrea Heugenhauser from Paris Lodron University Salzburg for all the helpful discussions on this topic.

Author contributions K.S.: Conception and design of the work, acquisition, analysis, interpretation of data, visualization, writing – original draft, review & editingD.B.: Conception and design of the work, interpretation of data, writing – review & editingB.M.: Conception and design of the work, writing – review & editing, supervision

Funding This work was funded by the German Federal Ministry of Economic Affairs and Climate Action (BMWK) and its Aviation Research Program "LuFo VI-1" ("MULTIKABIN", FKZ: 20Q1908C). Open Access funding enabled and organized by Projekt DEAL.

Compliance with ethical standards

Conflict of interest The authors declare no competing interests.

Publisher's note Springer Nature remains neutral with regard to jurisdictional claims in published maps and institutional affiliations.

References

1. Jiang J, Li Z, Li W et al. (2023) A review on insulation challenges towards electrification of aircraft. High. Volt. 8:209–230. https://doi.org/10.1049/hve2.12304
2. Bianco V, Manca O, Nardini S, Roma M (2009) Numerical investigation of transient thermal and fluidynamic fields in an executive aircraft cabin. Appl Therm. Eng. 29:3418–3425. https://doi.org/10.1016/j.applthermaleng.2009.05.020
3. Wu D, Wang Y, Gao Z, Yang J (2015) Insulation Performance of Heat-Resistant Material for High-Speed Aircraft Under Thermal Environments. J. Mater. Eng. Perform. 24:3373–3385. https://doi.org/10.1007/s11665-015-1626-7

4. Eze AH, Lakatos Á (2023) Applications of thermal insulation materials by aircraft. J. Phys: Conf. Ser. 2628:012018. https://doi.org/10.1088/1742-6596/2628/1/012018
5. Á Lakatos, AH Eze (2023) in Jármai K, Cservenák Á (eds) Vehicle and Automotive Engineering 4Springer International Publishing, Cham
6. Bheekhun N, Abu Talib AR, Hassan MR (2013) Aerogels in Aerospace: An Overview. Adv. Mater. Sci. Eng. 2013:1–18. https://doi.org/10.1155/2013/406065
7. SS Sonu, N Rai, I Chauhan (2023) J. Sol-Gel Sci. Technol. 105: 324–336. https://doi.org/10.1007/s10971-022-06026-1
8. McNeil SJ, Gupta H (2022) Emerging applications of aerogels in textiles. Polym. Test. 106:107426. https://doi.org/10.1016/j.polymertesting.2021.107426
9. Karamikamkar S, Naguib HE, Park CB (2020) Advances in precursor system for silica-based aerogel production toward improved mechanical properties, customized morphology, and multifunctionality: A review. Adv. Colloid Interface Sci. 276:102101. https://doi.org/10.1016/j.cis.2020.102101
10. T Budtova, T Lokki, S Malakooti, et al. (2022) Acoustic Properties of Aerogels: Current Status and Prospects, Adv. Eng. Mater. 25. https://doi.org/10.1002/adem.202201137
11. Shimizu T, Kanamori K, Nakanishi K (2017) Silicone-Based Organic–Inorganic Hybrid Aerogels and Xerogels. Chemistry 23:5176–5187. https://doi.org/10.1002/chem.201603680
12. Parale VG, Lee K-Y, Park H-H (2017) Flexible and Transparent Silica Aerogels: An Overview. J. Korean Ceram. Soc. 54:184–199. https://doi.org/10.4191/kcers.2017.54.3.12
13. Hayase G, Kanamori K, Nakanishi K (2011) New flexible aerogels and xerogels derived from methyltrimethoxysilane/dimethyldimethoxysilane co-precursors. J. Mater. Chem. 21:17077–17079. https://doi.org/10.1039/c1jm13664j
14. Ding J, Zhong K, Liu S et al. (2020) Flexible and super hydrophobic polymethylsilsesquioxane based silica aerogel for organic solvent adsorption via ambient pressure drying technique. Powder Technol. 373:716–726. https://doi.org/10.1016/j.powtec.2020.07.024
15. Luo Y, Li Z, Zhang W et al. (2019) Rapid synthesis and characterization of ambient pressure dried monolithic silica aerogels in ethanol/water co-solvent system. J. Non-Cryst. Solids 503-504:214–223. https://doi.org/10.1016/j.jnoncrysol.2018.09.049
16. Wu X, Zhong K, Ding J et al. (2020) Facile synthesis of flexible and hydrophobic polymethylsilsesquioxane based silica aerogel via the co-precursor method and ambient pressure drying technique. J. Non-Cryst. Solids 530:119826. https://doi.org/10.1016/j.jnoncrysol.2019.119826
17. Sert Çok S, Koç F, Dudás Z, Gizli N (2022) The Methyl Functionality of Monolithic Silica Xerogels Synthesized via the Co-Gelation Approach Combined with Surface Silylation. Gels 9:33. https://doi.org/10.3390/gels9010033
18. Hayase G, Kanamori K, Hasegawa G, Maeno A, Kaji H, Nakanishi K (2013) A superamphiphobic macroporous silicone monolith with marshmallow-like flexibility. Angew. Chem. Int Ed. Engl. 52:10788–10791. https://doi.org/10.1002/anie.201304169
19. Lei C, Hu Z, Zhang Y, Yang H, Li J, Hu S (2018) Tailoring structural and physical properties of polymethylsilsesquioxane aerogels by adjusting NH 3 ·H 2 O concentration. Microporous Mesoporous Mater. 258:236–243. https://doi.org/10.1016/j.micromeso.2017.05.009
20. Hayase G, Ohya Y (2017) Marshmallow-like silicone gels as flexible thermal insulators and liquid nitrogen retention materials and their application in containers for cryopreserved embryos. Appl Mater. Today 9:560–565. https://doi.org/10.1016/j.apmt.2017.10.004
21. R Fener, P Niemeyer, Flexible Komposite auf Basis von Aerogelen, European Patent EP3042884B1, 2023.
22. Emmerling A, Fricke J (1992) Small angle scattering and the structure of aerogels. J. Non-Cryst. Solids 145:113–120. https://doi.org/10.1016/s0022-3093(05)80439-9
23. U Schubert (2015) In: Levy D, Zayat M (ed) The Sol-Gel Handbook. Wiley-VCH Verlag GmbH & Co. KGaA, Weinheim
24. Venkateswara Rao A, Kulkarni MM, Amalnerkar DP, Seth T (2003) Superhydrophobic silica aerogels based on methyltrimethoxysilane precursor. J. Non-Cryst. Solids 330:187–195. https://doi.org/10.1016/j.jnoncrysol.2003.08.048
25. Bretz EA (2003) Putting humidity in its place. IEEE Spectr. 40:28–30. https://doi.org/10.1109/mspec.2003.1184443
26. Chen L, Wang S, Li G, Lin C-H, Zhang T (2016) CFD modeling of moisture accumulation in the insulation layers of an aircraft. Appl Therm. Eng. 102:1141–1156. https://doi.org/10.1016/j.applthermaleng.2016.04.048
27. Zhang T, Li G, Lin C-H, Wei Z, Wang S (2017) Experimental identification of key parameters contributing to moisture accumulation in an aircraft section. Build Environ. 126:339–347. https://doi.org/10.1016/j.buildenv.2017.10.012
28. Hrubesh LW, Pekala RW (1994) Thermal properties of organic and inorganic aerogels. J. Mater. Res. 9:731–738. https://doi.org/10.1557/jmr.1994.0731
29. Lu X, Arduini-Schuster MC, Kuhn J, Nilsson O, Fricke J, Pekala RW (1992) Thermal conductivity of monolithic organic aerogels. Science 255:971–972. https://doi.org/10.1126/science.255.5047.971
30. Wei G, Liu Y, Zhang X, Yu F, Du X (2011) Thermal conductivities study on silica aerogel and its composite insulation materials. Int J. Heat. Mass Transf. 54:2355–2366. https://doi.org/10.1016/j.ijheatmasstransfer.2011.02.026
31. Rege A, Voepel P, Okumus E, Hillgartner M, Itskov M, Milow B (2019) Temperature-Dependent Stiffening and Inelastic Behavior of Newly Synthesized Fiber-Reinforced Super Flexible Silica Aerogels. Mater. (Basel) 12:2878. https://doi.org/10.3390/ma12182878